



## OPEN Fuzzy-fractional modeling of cholera disease using real outbreak data of angola in caputo-TFN framework

Qursam Fatima<sup>1</sup>, Mubashir Qayyum<sup>1</sup>, Omar Khan<sup>2</sup>, Abdou Al zubaidi<sup>3</sup>, Syed Tauseef Saeed<sup>4</sup> & Jihad Younis<sup>5</sup>✉

Cholera is a waterborne disease that is mostly spread by taking tarnished food and water. This disease is brought on by bacteria *Vibrio cholerae* and causes infection in humans. The current manuscript proposes a fuzzy-fractional SEIHRD modeling framework for cholera disease outbreak in Angola using epidemiological data taken from World Health Organization. The Caputo fractional derivatives are used to capture the memory effects, while involved parameters are fuzzified using triangular fuzzy numbers for incorporating uncertainties involved in real-world data. The stability of the proposed model is examined to look at the circumstances in persistence and eradication of disease. For finding important factors influencing the dynamics of cholera transmission, sensitivity analysis is also carried out in this study. The effect of fractional and fuzzy parameters on the proposed model is analyzed via contour diagrams. The hybrid of fractional and fuzzy calculus yields a more realistic depiction of cholera dynamics, as depicted in numerical simulations. The analysis provides valuable results for planning public health initiatives for predicting and controlling cholera outbreaks.

**Keywords** Fuzzy-fractional modeling, Cholera Disease, Caputo fractional derivative, Triangular fuzzy number, Residual Power Series.

The bacterium *Vibrio cholerae* causes cholera, an infectious disease primarily transmitted through the consumption of contaminated food or water and, occasionally, through contact with bodily fluids from infected individuals<sup>1</sup>. Rivers, groundwater, and other aquatic environments contaminated with human feces provide ideal habitats for this pathogen, a comma-shaped, Gram-negative bacillus. In regions with poor sanitation infrastructure and inadequate sewage treatment, contaminated water supplies serve as major reservoirs of the bacterium, leading to frequent outbreaks<sup>2</sup>. After ingestion, the pathogen infects the human intestine, initiating a transmission cycle that releases vibrios back into the environment, where they can persist for extended periods even in the absence of human hosts<sup>3</sup>.

Historically, cholera has caused seven major pandemics since 1817. Recent large-scale outbreaks have been reported in Haiti (2010–2012), Yemen (2016–2020), and Zimbabwe (2008–2009)<sup>4–7</sup>. Although cholera is both preventable and treatable, it continues to pose a serious global health threat, with an estimated 1.3–4 million cases and 21,000–143,000 deaths annually worldwide<sup>8</sup>. The recurrence and increasing frequency of outbreaks highlight the urgent need for effective preventive measures, including improved hygiene, strong immunity, and accessible medical care. While oral cholera vaccines, such as Vaxchora, have demonstrated high short-term efficacy, their long-term effectiveness remains limited due to short protection duration and under utilization in low-resource settings<sup>9–12</sup>. Therefore, mathematical modeling serves as an essential tool for understanding transmission dynamics and enhancing intervention strategies.

Since the development of the classical SIR model by Kermack and McKendrick<sup>13</sup>, mathematical modeling has been a cornerstone in analyzing and predicting disease patterns to inform public health policies. Various modeling approaches have been employed to represent different pathways of cholera transmission, including compartmental and stochastic models developed under spatial, network-based, Bayesian, and machine learning

<sup>1</sup>Department of Sciences and Humanities, National University of Computer and Emerging Sciences Lahore Campus, Lahore, Pakistan. <sup>2</sup>Department of Computer Science, National University of Computer and Emerging Sciences Peshawar Campus, Peshawar, Pakistan. <sup>3</sup>Department of Mathematics, College of Science, King Khalid University, Abha 61413, Saudi Arabia. <sup>4</sup>Department of Mathematics and Statistics, The University of Lahore, Lahore, Pakistan. <sup>5</sup>Department of Mathematics, Aden University, Aden, Yemen. ✉email: jihadalsaqqaf@gmail.com

frameworks<sup>1,14–17</sup>. To improve understanding of disease dynamics, these models have been extended to account for the environmental persistence of the pathogen<sup>18</sup> and population heterogeneity in transmission patterns<sup>19</sup>.

Despite these advancements, most classical models still rely on deterministic frameworks and assume homogeneity among parameters, limiting their ability to capture the inherent randomness and variability observed in real-world data. This limitation arises from underreporting of outbreaks and variations in population behavior, such as differences in transmission and recovery rates or contact patterns. However, a significant research gap remains in integrating both parameter uncertainty and memory-dependent effects within a unified cholera modeling framework, particularly using real WHO outbreak data. Existing studies have largely examined fuzziness and fractional dynamics independently, leaving the combined impact of these effects on cholera transmission insufficiently explored.

To address this gap, the present study incorporates fuzzy set theory into epidemic modeling, a concept first introduced by Zadeh<sup>20</sup>. This allows uncertain epidemiological parameters to be represented using fuzzy numbers<sup>21,22</sup>. Simultaneously, fractional calculus has gained considerable attention for its ability to capture memory effects in biological systems, providing a natural generalization of classical differential operators<sup>23</sup>. This approach has been effectively applied in modeling infectious disease transmission<sup>24–34</sup>, population dynamics<sup>35</sup>, and tumor growth<sup>36,37</sup>.

By combining fuzzy and fractional calculus, fuzzy-fractional differential systems provide a powerful framework for modeling disease dynamics under both uncertainty and memory effects. Motivated by this, the present study proposes a fuzzy-fractional SEIHRD model for cholera. The model employs triangular fuzzy numbers to represent uncertainty in epidemiological parameters and applies the Caputo fractional derivative to capture the memory effect in disease transmission. Using recent WHO-reported data from the Angola outbreak, the proposed model is numerically solved via a fuzzy-fractional extension of the Laplace Residual Power Series Method (LRPSM), and its stability around the disease-free equilibrium is analyzed. This generalized framework provides new insights into cholera dynamics and offers a robust approach for designing effective public health interventions, particularly in resource-limited, high-risk environments.

## Preliminaries

**Definition 1**<sup>38</sup> The Caputo fractional derivative of order  $\omega$  for a function  $\psi(t)$ , denoted by  ${}^C D_t^\omega$ , is given as

$${}^C D_t^\omega \psi(t) = \frac{1}{\Gamma(n-\omega)} \int_0^t (t-\xi)^{n-\omega-1} \psi^{(n)}(\xi) d\xi, \quad n-1 < \omega \leq n, \quad (1)$$

where  $n = \lceil \omega \rceil$  and  $\Gamma(\cdot)$  represents the Gamma function.

**Definition 2** Consider a function  $\psi(t)$  that is piecewise continuous and of exponential order  $\delta$  on the interval  $[0, \infty)$ . Its Laplace transform is defined as

$$\Psi(s) = \mathcal{L}[\psi(t)] = \int_0^\infty e^{-st} \psi(t) dt, \quad s > \delta. \quad (2)$$

The inverse Laplace transform is expressed as

$$\psi(t) = \mathcal{L}^{-1}[\Psi(s)] = \frac{1}{2\pi i} \int_{c-i\infty}^{c+i\infty} e^{st} \Psi(s) ds, \quad c > \text{Re}(s_0), \quad (3)$$

where  $\text{Re}(s_0)$  denotes the real part of the rightmost singularity of  $\Psi(s)$ .

**Lemma**<sup>39</sup> Let  $\psi(t)$  and  $\phi(t)$  be piecewise continuous on  $[0, \infty)$ , and let  $a, b \in \mathbb{R}$ . The Laplace transform has the following properties:

- $\mathcal{L}[a\psi(t) + b\phi(t)] = a\Psi(s) + b\Phi(s)$ ,
- $\mathcal{L}^{-1}[a\Psi(s) + b\Phi(s)] = a\psi(t) + b\phi(t)$ ,
- $\lim_{s \rightarrow \infty} s\Psi(s) = \psi(0)$ ,
- $\mathcal{L}[t^\omega] = \frac{\Gamma(\omega+1)}{s^{\omega+1}}, \quad \omega > -1$ ,
- $\mathcal{L}[{}^C D_t^\omega \psi(t)] = s^\omega \Psi(s) - \sum_{k=0}^{n-1} s^{\omega-k-1} \psi^{(k)}(0), \quad n-1 < \omega < n$ .

**Definition 3**<sup>38</sup> Let  $\mathbb{R}$  denote the set of real numbers. A fuzzy set  $\tilde{F} \subset \mathbb{R}$  is characterized by a membership function  $\mu_{\tilde{F}} : \mathbb{R} \rightarrow [0, 1]$ . Its  $p$ -level set (also called the  $p$ -cut) is defined as

$$[\tilde{F}]^p = \{x \in \mathbb{R} : \mu_{\tilde{F}}(x) \geq p\}, \quad p \in [0, 1].$$

A fuzzy set  $\tilde{F}$  qualifies as a *fuzzy number* if it satisfies:

- Normality:** There exists  $x_0 \in \mathbb{R}$  with  $\mu_{\tilde{F}}(x_0) = 1$ ,
- Convexity:** For all  $x_1, x_2 \in \mathbb{R}$  and  $\lambda \in [0, 1]$ ,

$$\mu_{\tilde{F}}(\lambda x_1 + (1-\lambda)x_2) \geq \min\{\mu_{\tilde{F}}(x_1), \mu_{\tilde{F}}(x_2)\},$$

3. **Upper semi-continuity** of  $\mu_{\tilde{F}}$ ,
4. Compactness of the closure of  $\{x \in \mathbb{R} : \mu_{\tilde{F}}(x) > 0\}$ .

**Definition 4**<sup>38</sup> A *triangular fuzzy number (TFN)*  $\tilde{F}$  is represented by a triplet  $(u, v, z)$  with  $u < v < z$ . Its membership function is given by

$$\mu_{\tilde{F}}(x) = \begin{cases} 0, & x \leq u, \\ \frac{x-u}{v-u}, & u \leq x \leq v, \\ \frac{z-x}{z-v}, & v \leq x \leq z, \\ 0, & x \geq z. \end{cases}$$

The corresponding  $p$ -level set is

$$[\tilde{F}]^p = [u + (v - u)p, z - (z - v)p], \quad p \in [0, 1], \tag{4}$$

where the interval bounds denote the lower and upper limits of  $\tilde{F}$  at level  $p$ .

**Definition 5**<sup>38</sup> A fuzzy number  $\tilde{F}(p)$  can also be expressed in parametric form as

$$\tilde{F}(p) = [\underline{F}(p), \overline{F}(p)],$$

where

1.  $\underline{F}(p)$  is left-continuous, bounded, and non-decreasing,
2.  $\overline{F}(p)$  is left-continuous, bounded, and non-increasing,
3.  $\underline{F}(p) \leq \overline{F}(p)$  holds for all  $p \in [0, 1]$ .

### Cholera disease model transmission

*Vibrio cholerae* is the bacterium that causes cholera, a highly contagious waterborne infection that causes severe dehydration and acute watery diarrhea, both of which can be fatal if left untreated. The main method of transmission is by consuming food or drink tainted with an infected person’s excrement. Because cholera spreads through inadequate sanitation, contaminated water supplies, and poor hygiene, it is more likely in regions with high population densities or disasters than directly transmitted viral illnesses. In past cholera epidemics in Asia and Africa bring out that how important it is to document the transmission dynamics of diseases for control and effective treatment of public.

With the use of Angola outbreak data taken from World Health Organization (WHO), we develop a compartmental model to analyze disease transmission and control of cholera. Biological description along with parameter values are presented in Table 1, while disease flow diagram is given in Fig. 1. Total population  $\mathcal{N}(t)$  is divided into six epidemiological states, i.e. susceptible ( $\mathcal{S}(t)$ ), exposed ( $\mathcal{E}(t)$ ), infectious ( $\mathcal{I}(t)$ ), hospitalized ( $\mathcal{H}(t)$ ), recovered ( $\mathcal{R}(t)$ ), and the disease-induced deaths  $\mathcal{D}(t)$ . Therefore, the entire population is satisfied with

$$\mathcal{N}(t) = \mathcal{S}(t) + \mathcal{E}(t) + \mathcal{I}(t) + \mathcal{H}(t) + \mathcal{R}(t) + \mathcal{D}(t).$$

According to this formulation, susceptible individuals contract the disease at a transmission rate  $\alpha$  with contaminated food or water. They move to the infectious stage with a rate  $\eta$  during the incubation period after becoming infected and entering the exposed class. The recovery rate of infectious individuals is  $\lambda$ , the rate of hospitalization is  $\sigma$ , and rate of death from severe dehydration is  $\rho$ . Patients in hospitals may die at a rate of  $\tau$  or

Parameters	Description	Values	References
$\Omega$	Recruitment rate	$1.03 \times 10^{-4}$ per capita	Calculated
$\alpha$	Transmission rate	1.076	Estimated
$\eta$	Rate of progression from exposed to infectious (1/incubation period)	1/10 per day	<sup>42</sup>
$\lambda$	Recovery rate of infectious individuals	0.9615 per day	<sup>42</sup>
$\rho$	Death rate of infectious individuals	0.0385 per day	<sup>42</sup>
$\sigma$	Hospitalization rate of infectious individuals	0.0296 per day	<sup>42</sup>
$\theta$	Recovery rate of hospitalized individuals	0.975 per day	<sup>42</sup>
$\tau$	Death rate of hospitalized individuals	0.025 per day	<sup>42</sup>
$\xi$	Natural death rate	$9.46 \times 10^{-5}$ per capita	Calculated

**Table 1.** Biological description and values of parameters for cholera model. All parameter values were obtained from WHO-reported cholera data, and the fuzzy ranges were defined as  $\pm 10\%$  of the baseline values to account for data variability, reporting uncertainty, and regional fluctuations in transmission and recovery rates.

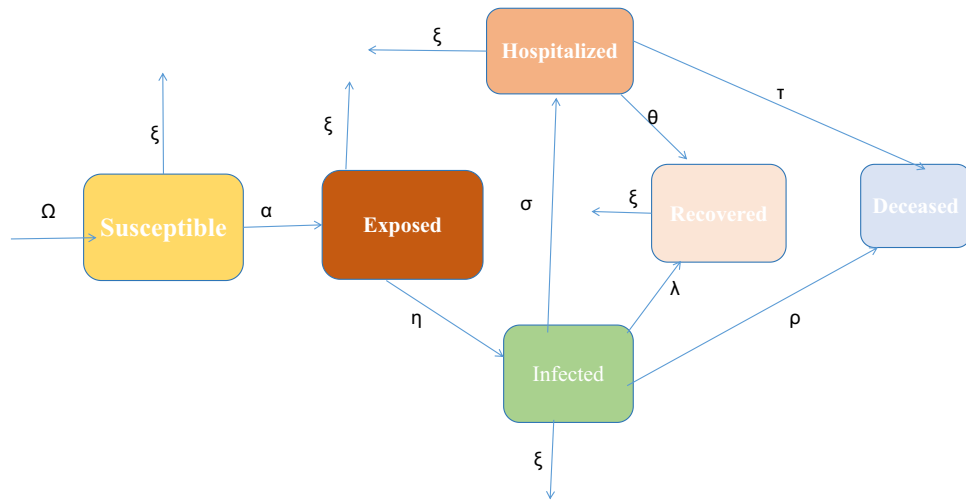


**Figure 1.** Flow diagram of the SEIHRD model for Cholera transmission dynamics, illustrating the transitions among the Susceptible (S), Exposed (E), Infected (I), Hospitalized (H), Recovered (R), and Deceased (D) compartments with all relevant parameters.

recovered at a rate of  $\theta$ . It is believed that recovered individuals develop long-lasting protection against cholera, even though deaths are reported separately.

The model is governed by the following system of differential equations:

$$\begin{aligned}
 \mathbb{D}_t \mathbb{S}(t) &= \Omega - \alpha \mathbb{S} \frac{\mathbb{I}}{\mathcal{N}} - \xi \mathbb{S} \\
 \mathbb{D}_t \mathbb{E}(t) &= \alpha \mathbb{S} \frac{\mathbb{I}}{\mathcal{N}} - (\eta + \xi) \mathbb{E} \\
 \mathbb{D}_t \mathbb{I}(t) &= \eta \mathbb{E} - (\lambda + \rho + \sigma + \xi) \mathbb{I} \\
 \mathbb{D}_t \mathbb{H}(t) &= \sigma \mathbb{I} - (\theta + \tau + \xi) \mathbb{H} \\
 \mathbb{D}_t \mathbb{R}(t) &= \lambda \mathbb{I} + \theta \mathbb{H} - \xi \mathbb{R} \\
 \mathbb{D}_t \mathbb{D}(t) &= \rho \mathbb{I} + \tau \mathbb{H}
 \end{aligned}
 \tag{5}$$

subject to the initial conditions:

$$\mathbb{S}(0) = S_0 \geq 0, \quad \mathbb{E}(0) = E_0 \geq 0, \quad \mathbb{I}(0) = I_0 \geq 0, \quad \mathbb{H}(0) = H_0 \geq 0, \quad \mathbb{R}(0) = R_0 \geq 0, \quad \mathbb{D}(0) = D_0 \geq 0.$$

### Solution positivity

**Lemma 1** <sup>40</sup> Let  $Y(t) = (\mathbb{S}(t), \mathbb{E}(t), \mathbb{I}(t), \mathbb{H}(t), \mathbb{R}(t), \mathbb{D}(t))$  denote the solution of the Cholera Disease model governed by system (1), subject to non-negative initial conditions  $Y(0) \geq 0$ . Then the model possesses the following properties:

1. All compartment populations remain non-negative for all  $t > 0$ ; that is,  $Y(t) \geq 0$ .
2. The total living population  $\mathbb{P}(t) = \mathbb{S}(t) + \mathbb{E}(t) + \mathbb{I}(t) + \mathbb{H}(t) + \mathbb{R}(t)$  satisfies:

$$\lim_{t \rightarrow \infty} \mathbb{P}(t) \leq \frac{\Omega}{\xi}.$$

**Proof** Assume  $t^* = \sup\{t > 0 : Y(t) > 0 \text{ on } [0, t]\}$  and suppose  $t^* > 0$ . We analyze the system to establish positivity.

For the susceptible population  $\mathbb{S}(t)$ , we have:

$$\frac{d\mathbb{S}}{dt} = \Omega - \alpha \mathbb{S} \mathbb{I} - \xi \mathbb{S}.$$

Letting  $\omega(t) = \alpha \mathbb{I}(t)$ , this can be rewritten as:

$$\frac{d\mathbb{S}}{dt} = \Omega - (\omega(t) + \xi) \mathbb{S}(t).$$

Multiplying by the integrating factor  $\exp\left(\xi t + \int_0^t \omega(\tau) d\tau\right)$ , we obtain:

$$\frac{d}{dt} \left[ \mathbb{S}(t) \exp\left(\xi t + \int_0^t \omega(\tau) d\tau\right) \right] = \Omega \exp\left(\xi t + \int_0^t \omega(\tau) d\tau\right).$$

Integrating over  $[0, t^*]$ , we have:

$$\begin{aligned} \mathbb{S}(t^*) &= \mathbb{S}(0) \exp\left(-\xi t^* - \int_0^{t^*} \omega(q) dq\right) \\ &+ \exp\left(-\xi t^* - \int_0^{t^*} \omega(q) dq\right) \int_0^{t^*} \Omega \exp\left(\xi x + \int_0^x \omega(f) df\right) dx > 0. \end{aligned}$$

Since  $\mathbb{S}(0) \geq 0$  and  $\Omega > 0$ , it follows that  $\mathbb{S}(t) \geq 0$  for all  $t > 0$ .

Using the same approach for  $\mathbb{E}(t)$ ,  $\mathbb{I}(t)$ ,  $\mathbb{H}(t)$ ,  $\mathbb{R}(t)$ ,  $\mathbb{F}(t)$ , we conclude that:

$$\mathbb{E}(t), \mathbb{I}(t), \mathbb{H}(t), \mathbb{R}(t), \mathbb{F}(t) \geq 0 \quad \text{for all } t > 0.$$

Next, define the total living population:

$$\mathbb{P}(t) = \mathbb{S}(t) + \mathbb{E}(t) + \mathbb{I}(t) + \mathbb{H}(t) + \mathbb{R}(t).$$

Summing the first five equations yields:

$$\frac{d\mathbb{P}}{dt} = \Omega - \xi \mathbb{P}(t) - \rho \mathbb{I}(t) - \tau \mathbb{H}(t) \leq \Omega - \xi \mathbb{P}(t).$$

Solving this inequality gives:

$$\lim_{t \rightarrow \infty} \mathbb{P}(t) \leq \frac{\Omega}{\xi}.$$

This completes the proof.

### Stability analysis of the disease-free case for cholera disease

This section analyzes the stability of the Cholera Disease model at the disease-free equilibrium (DFE). By setting the right-hand sides of the model equations to zero, we obtain the DFE as:

$$E_0 = \left( \frac{\Omega}{\xi}, 0, 0, 0, 0 \right).$$

To calculate the basic reproduction number  $\mathcal{R}_0$ , we apply the next generation matrix approach<sup>41</sup>, focusing on the infected compartments: exposed  $\mathbb{E}$ , infected  $\mathbb{I}$ , and hospitalized  $\mathbb{H}$ .

The corresponding matrices  $F$  and  $V$  are given by:

$$F = \begin{pmatrix} 0 & \alpha \frac{\Omega}{\xi} & 0 \\ 0 & 0 & 0 \\ 0 & 0 & 0 \end{pmatrix}$$

Since

$$V = \begin{pmatrix} k_1 & 0 & 0 \\ -\eta & k_2 & 0 \\ 0 & -\sigma & k_3 \end{pmatrix}, \quad k_1 = \eta + \xi, \quad k_2 = \lambda + \rho + \sigma + \xi, \quad k_3 = \theta + \tau + \xi,$$

the inverse of  $V$  is :

$$V^{-1} = \begin{pmatrix} \frac{1}{k_1} & 0 & 0 \\ \frac{\eta}{k_1 k_2} & \frac{1}{k_2} & 0 \\ \frac{\eta \sigma}{k_1 k_2 k_3} & \frac{\sigma}{k_2 k_3} & \frac{1}{k_3} \end{pmatrix}.$$

Now compute

$$FV^{-1} = \begin{pmatrix} 0 & \frac{\alpha\Omega}{\xi} & 0 \\ 0 & 0 & 0 \\ 0 & 0 & 0 \end{pmatrix} \begin{pmatrix} \frac{1}{k_1} & 0 & 0 \\ \frac{\eta}{k_1 k_2} & \frac{1}{k_2} & 0 \\ \frac{\eta\sigma}{k_1 k_2 k_3} & \frac{k_2}{k_2 k_3} & \frac{1}{k_3} \end{pmatrix} = \begin{pmatrix} \frac{\alpha\Omega\eta}{\xi k_1 k_2} & \frac{\alpha\Omega}{\xi k_2} & 0 \\ 0 & 0 & 0 \\ 0 & 0 & 0 \end{pmatrix}.$$

The spectral radius of  $FV^{-1}$  is

$$\mathcal{R}_0 = \frac{\alpha\Omega\eta}{\xi k_1 k_2}.$$

**Interpretation:** The disease-free equilibrium is locally asymptotically stable if  $\mathcal{R}_0 < 1$ , and unstable if  $\mathcal{R}_0 > 1$ .

**Theorem 1** *The disease-free equilibrium (DFE)  $E_0 = (\frac{\Omega}{\xi}, 0, 0, 0, 0, 0)$  of the Cholera Disease model is locally asymptotically stable if  $\mathcal{R}_0 < 1$ .*

**Proof** To prove the theorem, we first evaluate the Jacobian matrix of the system at the disease-free equilibrium. The compartments are: susceptible  $\mathbb{S}$ , exposed  $\mathbb{E}$ , infected  $\mathbb{I}$ , hospitalized  $\mathbb{H}$ , recovered  $\mathbb{R}$ , and fatalities  $\mathbb{F}$ .

The Jacobian matrix at  $E_0$  is:

$$J = \begin{bmatrix} -\xi & -\alpha\frac{\Omega}{\xi} & 0 & 0 & 0 & 0 \\ 0 & -k_1 & \alpha\frac{\Omega}{\xi} & 0 & 0 & 0 \\ 0 & \eta & -k_2 & 0 & 0 & 0 \\ 0 & 0 & \sigma & -k_3 & 0 & 0 \\ 0 & 0 & \lambda & \theta & -\xi & 0 \\ 0 & 0 & \rho & \tau & 0 & 0 \end{bmatrix}$$

with:

$$k_1 = \eta + \xi, \quad k_2 = \lambda + \rho + \sigma + \xi, \quad k_3 = \theta + \tau + \xi.$$

The eigenvalues are:

$$\lambda_1 = -\xi, \quad \lambda_2 = -\xi, \quad \lambda_3 = -k_3,$$

which are negative.

For the infected subsystem ( $\mathbb{E}, \mathbb{I}, \mathbb{H}$ ), the reduced Jacobian block is:

$$J_{\text{infected}} = \begin{bmatrix} -k_1 & \alpha\frac{\Omega}{\xi} & 0 \\ \eta & -k_2 & 0 \\ 0 & \sigma & -k_3 \end{bmatrix}$$

The characteristic equation is:

$$\lambda^3 + b_1\lambda^2 + b_2\lambda + b_3 = 0$$

with:

$$\begin{aligned} b_1 &= k_1 + k_2 + k_3, \\ b_2 &= k_1 k_2 + k_1 k_3 + k_2 k_3, \\ b_3 &= k_1 k_2 k_3 (1 - \mathcal{R}_0). \end{aligned}$$

The basic reproduction number is:

$$\mathcal{R}_0 = \frac{\alpha\Omega\eta}{\xi k_1 k_2}.$$

If  $\mathcal{R}_0 < 1$ , then: - All coefficients  $b_1, b_2, b_3 > 0$  - Applying Routh-Hurwitz: Since  $b_1 b_2 > b_3$ , stability holds. Thus, the DFE is locally asymptotically stable when  $\mathcal{R}_0 < 1$ .

### Stability analysis of the endemic case for cholera disease

This section presents the endemic equilibrium point (EE) and its stability analysis. At endemic equilibrium, all derivatives vanish and the infected population persists ( $\mathbb{I}^* > 0$ ). Solving the steady-state system yields the endemic equilibrium:

$$E^* = (\mathbb{S}^*, \mathbb{E}^*, \mathbb{I}^*, \mathbb{H}^*, \mathbb{R}^*, \mathbb{D}^*),$$

where

$$\begin{aligned} \mathbb{I}^* &= \frac{\Omega(\mathcal{R}_0 - 1)}{\alpha - \Psi}, & \Psi &= \rho + \frac{\tau\sigma}{\theta + \tau + \xi}, \\ \mathbb{H}^* &= \frac{\sigma}{\theta + \tau + \xi} \mathbb{I}^*, & \mathbb{E}^* &= \frac{\lambda + \rho + \sigma + \xi}{\eta} \mathbb{I}^*, \\ \mathbb{R}^* &= \frac{\lambda \mathbb{I}^* + \theta \mathbb{H}^*}{\xi}, & \mathcal{N}^* &= \frac{\Omega - \Psi \mathbb{I}^*}{\xi}, & \mathbb{S}^* &= \frac{\mathcal{N}^*}{\mathcal{R}_0}. \end{aligned}$$

**Existence condition:** The endemic equilibrium exists when  $\mathcal{R}_0 > 1$  and  $\alpha > \Psi$ , ensuring positivity of all equilibrium components.

**Theorem 2** *The endemic equilibrium (EE) of the Cholera Disease model is locally asymptotically stable if  $\mathcal{R}_0 > 1$ .*

**Proof** We evaluate the Jacobian of the system at the endemic equilibrium  $E^*$ . The Jacobian has a block triangular form where the submatrix corresponding to recovered and hospitalized compartments yields strictly negative eigenvalues (since diagonal entries are  $-(\theta + \tau + \xi)$  and  $-\xi$ ).

The infection subsystem  $(\mathbb{E}, \mathbb{I})$  produces the characteristic polynomial

$$\lambda^2 + c_1\lambda + c_2 = 0,$$

with coefficients

$$c_1 = (\eta + \xi) + (\lambda + \rho + \sigma + \xi) > 0, \quad c_2 = (\eta + \xi)(\lambda + \rho + \sigma + \xi)(\mathcal{R}_0 - 1).$$

Since  $\mathcal{R}_0 > 1$ , both coefficients are positive, implying negative real parts of the roots. Hence, by the Routh–Hurwitz criterion, all eigenvalues of the Jacobian at the endemic equilibrium are negative.

**Conclusion:** The endemic equilibrium exists when  $\mathcal{R}_0 > 1$  and  $\alpha > \Psi$ , and it is locally asymptotically stable under these conditions.

### Existence and uniqueness theorem for the cholera disease model

Consider the Cholera Disease model governed by the following system of ordinary differential equations. Let the state vector be

$$z(t) = \begin{pmatrix} \mathbb{S}(t) \\ \mathbb{E}(t) \\ \mathbb{I}(t) \\ \mathbb{H}(t) \\ \mathbb{R}(t) \\ \mathbb{D}(t) \end{pmatrix}, \quad \mathcal{N}(t) = \mathbb{S}(t) + \mathbb{E}(t) + \mathbb{I}(t) + \mathbb{H}(t) + \mathbb{R}(t).$$

The system can be written in compact form as

$$\frac{dz}{dt} = g(t, z),$$

where

$$g(t, z) = \begin{pmatrix} \Omega - \alpha \frac{\mathbb{S}(t)\mathbb{I}(t)}{\mathcal{N}(t)} - \xi \mathbb{S}(t) \\ \alpha \frac{\mathbb{S}(t)\mathbb{I}(t)}{\mathcal{N}(t)} - (\eta + \xi)\mathbb{E}(t) \\ \eta \mathbb{E}(t) - (\lambda + \rho + \sigma + \xi)\mathbb{I}(t) \\ \sigma \mathbb{I}(t) - (\theta + \tau + \xi)\mathbb{H}(t) \\ \lambda \mathbb{I}(t) + \theta \mathbb{H}(t) - \xi \mathbb{R}(t) \\ \rho \mathbb{I}(t) + \tau \mathbb{H}(t) \end{pmatrix}.$$

**Continuity:** Each component of  $g(t, z)$  is a rational function with denominator  $\mathcal{N}(t)$ . On the biologically relevant domain where  $\mathcal{N}(t) > 0$ , all terms are continuous in both  $t$  and  $z$ . Therefore,  $g(t, z)$  is continuous in any neighborhood containing the initial condition  $(t_0, z_0)$ .

**Local Lipschitz Condition:** To establish uniqueness, we verify that  $g(t, z)$  satisfies a local Lipschitz condition with respect to  $z$ . The Jacobian matrix of  $g$  with respect to  $z$  is

$$D_z g(t, z) = \begin{pmatrix} -\alpha \frac{I}{N} - \xi & 0 & -\alpha \frac{S}{N} + \alpha \frac{SI}{N^2} & 0 & 0 & 0 \\ \alpha \frac{I}{N} & -(\eta + \xi) & \alpha \frac{S}{N} - \alpha \frac{SI}{N^2} & 0 & 0 & 0 \\ 0 & \eta & -(\lambda + \rho + \sigma + \xi) & 0 & 0 & 0 \\ 0 & 0 & \sigma & -(\theta + \tau + \xi) & 0 & 0 \\ 0 & 0 & \lambda & \theta & -\xi & 0 \\ 0 & 0 & \rho & \tau & 0 & 0 \end{pmatrix}.$$

The entries of this Jacobian are continuous and bounded on any compact subset of  $\mathbb{R}^6$  with  $N > 0$ . Therefore, there exists a constant  $K > 0$  such that

$$\|g(t, z_1) - g(t, z_2)\| \leq K \|z_1 - z_2\|, \quad \forall z_1, z_2 \in \mathcal{D},$$

where  $\mathcal{D}$  is a compact domain containing the initial data. This confirms that  $g$  is locally Lipschitz in  $z$ .

**Application of Cauchy-Lipschitz Theorem:** Since the right-hand side  $g(t, z)$  is continuous in  $t$  and locally Lipschitz in  $z$ , the hypotheses of the Cauchy-Lipschitz (Picard-Lindelöf) theorem are satisfied. Consequently, there exists a unique local solution  $z(t)$  to the initial value problem

$$\frac{dz}{dt} = g(t, z), \quad z(t_0) = z_0,$$

on some interval  $[t_0 - \epsilon, t_0 + \epsilon]$ , where  $\epsilon > 0$  depends on the local properties of  $g$ .

**Global Existence:** Because  $g$  is locally Lipschitz and solutions remain bounded in the invariant set above, the local solution extends to all  $t \geq 0$ . This establishes global existence and uniqueness.

**Conclusion:** Thus, the Cholera Disease model admits a unique global solution for any given nonnegative initial conditions with  $N(0) > 0$ .

### Fuzzy-fractional modeling of the cholera disease

The bacteria *Vibrio cholerae* is the cause of cholera, a serious waterborne illness that can be fatal if untreated. It is characterized by acute watery diarrhea and dehydration. It is particularly common in places with poor cleanliness or tainted drinking water sources. Cholera spread quickly and can cause large scale outbreak, especially in those areas having limited resources. Due to this reason, it is important to accurately capture the dynamics of cholera transmission for effective prevention and control measures. In this regard, proposing fuzzy-fractional SEIHRD model for cholera is the main goal of this section. By applying Caputo fractional derivatives the modified cholera SEIHRD system is defined using Definition 1 as:

$$\begin{aligned} CD_t^\omega S(t) &= \Omega - \alpha S \frac{I}{N} - \xi S \\ CD_t^\omega E(t) &= \alpha S \frac{I}{N} - (\eta + \xi) E \\ CD_t^\omega I(t) &= \eta E - (\lambda + \rho + \sigma + \xi) I \\ CD_t^\omega H(t) &= \sigma I - (\theta + \tau + \xi) H \\ CD_t^\omega R(t) &= \lambda I + \theta H - \xi R \\ CD_t^\omega D(t) &= \rho I + \tau H \end{aligned}$$

where  $\omega$  represents the fractional order of the derivative in the Caputo sense and satisfies  $\omega \in (0, 1]$ . To capture uncertainty associated with real data on cholera, triangular fuzzy numbers (TFNs) are introduced in the involved parameters as:

$$\begin{aligned} \tilde{\alpha} &= [0.8608 + (1.076 - 0.8608)r, 1.2912 - (1.2912 - 1.076)r], \\ \tilde{\eta} &= [0.08 + (0.1 - 0.08)r, 0.12 - (0.12 - 0.1)r], \\ \tilde{\lambda} &= [0.7692 + (0.9615 - 0.7692)r, 1.1538 - (1.1538 - 0.9615)r], \\ \tilde{\sigma} &= [0.0237 + (0.0296 - 0.0237)r, 0.0355 - (0.0355 - 0.0296)r], \\ \tilde{\theta} &= [0.780 + (0.975 - 0.780)r, 1.179 - (1.179 - 0.975)r] \end{aligned} \tag{7}$$

Thus, the fuzzy-fractional model for cholera disease takes the form:

$$\begin{aligned}
 CD_t^\omega \tilde{S}(t, p) &= \Omega - \tilde{\alpha} \tilde{S}(p, t) \frac{\tilde{I}(p, t)}{\mathcal{N}} - \xi \tilde{S}(p, t), \\
 CD_t^\omega \tilde{E}(t, p) &= \tilde{\alpha} \tilde{S}(p, t) \frac{\tilde{I}(p, t)}{\mathcal{N}} - (\tilde{\eta} + \xi) \tilde{E}(p, t), \\
 CD_t^\omega \tilde{I}(t, p) &= \tilde{\eta} \tilde{E}(p, t) - (\tilde{\lambda} + \rho + \tilde{\sigma} + \xi) \tilde{I}(p, t), \\
 CD_t^\omega \tilde{H}(t, p) &= \tilde{\sigma} \tilde{I}(p, t) - (\tilde{\theta} + \tau + \xi) \tilde{H}(p, t), \\
 CD_t^\omega \tilde{R}(t, p) &= \tilde{\lambda} \tilde{I}(p, t) + \tilde{\theta} \tilde{H}(p, t) - \xi \tilde{R}(p, t), \\
 CD_t^\omega \tilde{D}(t, p) &= \rho \tilde{I}(p, t) + \tau \tilde{H}(p, t),
 \end{aligned} \tag{8}$$

with fuzzy initial conditions

$$\tilde{S}(0) = \mathbb{B}_{1,0}, \quad \tilde{E}(0) = \mathbb{B}_{2,0}, \quad \tilde{I}(0) = \mathbb{B}_{3,0}, \quad \tilde{H}(0) = \mathbb{B}_{4,0}, \quad \tilde{R}(0) = \mathbb{B}_{3,0}, \quad \tilde{D}(0) = \mathbb{B}_{4,0}. \tag{9}$$

### Importance of modeling cholera as fuzzy-fractional system

Fuzzy-fractional modeling of cholera dynamics is important because memory effects are essential to actual epidemic dynamics. On the other hand, fuzzy numbers make it possible to incorporate uncertainty into epidemiological data. This is needed in those areas where trustworthy surveillance systems is not installed. The fuzzy-fractional model provides a more realistic framework for capturing cholera disease by integrating different methods. Reduction of cholera in susceptible groups, allocating healthcare resources, and efficient control measures, all depend on this enhanced prediction capability.

### Analytical solution of the fuzzy-fractional SEIHRD model via the laplace residual power series method

In this section, we apply Laplace Residual Power Series (LRPS) method to obtain series form solutions of fuzzy-fractional SEIHRD model given in (8) and (9). The model consists of six main compartments representing the susceptible ( $\tilde{S}(p, t)$ ), exposed ( $\tilde{E}(p, t)$ ), infected ( $\tilde{I}(p, t)$ ), hospitalized ( $\tilde{H}(p, t)$ ), recovered ( $\tilde{R}(p, t)$ ), and deceased ( $\tilde{D}(p, t)$ ) populations.

We represent each fuzzy solution  $\tilde{Y}(p, t)$  in parametric form as:

$$\tilde{Y}(p, t) = [\underline{\tilde{Y}}(p, t), \overline{\tilde{Y}}(p, t)],$$

where  $\underline{\tilde{Y}}$  and  $\overline{\tilde{Y}}$  denote the lower and upper bounds of the fuzzy solution, respectively.

**Step 1:** Applying the Laplace transform to each fuzzy-fractional equation yields:

$$\begin{aligned}
 \tilde{S}(s, p) &= \frac{\tilde{S}_0}{s} - \frac{1}{s^\omega} \left[ \frac{\Omega}{s} + \mathcal{L} \left( \tilde{\alpha} \cdot \mathcal{L}^{-1} \left( \frac{\tilde{I}}{\mathcal{N}} \right) \cdot \mathcal{L}^{-1}(\tilde{S}) \right) + \xi \tilde{S}(s, p) \right], \\
 \tilde{E}(s, p) &= \frac{\tilde{E}_0}{s} - \frac{1}{s^\omega} \left[ \mathcal{L} \left( \tilde{\alpha} \cdot \mathcal{L}^{-1} \left( \frac{\tilde{I}}{\mathcal{N}} \right) \cdot \mathcal{L}^{-1}(\tilde{S}) \right) + (\xi + \tilde{\eta}) \tilde{E}(s, p) \right], \\
 \tilde{I}(s, p) &= \frac{\tilde{I}_0}{s} - \frac{1}{s^\omega} \left[ \tilde{\eta} \tilde{E}(s, p) + (\xi + \lambda + \rho + \sigma) \tilde{I}(s, p) \right], \\
 \tilde{H}(s, p) &= \frac{\tilde{H}_0}{s} - \frac{1}{s^\omega} \left[ \tilde{\sigma} \tilde{I}(s, p) + (\theta + \tau + \xi) \tilde{H}(s, p) \right], \\
 \tilde{R}(s, p) &= \frac{\tilde{R}_0}{s} - \frac{1}{s^\omega} \left[ \lambda \tilde{I}(s, p) + \tilde{\theta} \tilde{H}(s, p) + \xi \tilde{R}(s, p) \right], \\
 \tilde{D}(s, p) &= \frac{\tilde{D}_0}{s} - \frac{1}{s^\omega} \left[ \rho \tilde{I}(s, p) + \tau \tilde{H}(s, p) \right].
 \end{aligned}$$

**Step 2:** Let each fuzzy compartment be approximated by the truncated fractional power series:

$$\tilde{Y}_k(s, p) = \sum_{n=0}^k \tilde{Y}_n s^{-(n\omega+1)}, \quad \text{for } \tilde{Y} \in \{\tilde{S}, \tilde{E}, \tilde{I}, \tilde{H}, \tilde{R}, \tilde{D}\}.$$

**Step 3:** The  $k^{\text{th}}$  Laplace residual function for the susceptible class, for example, is:

$$LRes(\tilde{S}_k) = \tilde{S}_k(s, p) - \frac{\tilde{S}_0}{s} + \frac{1}{s^\omega} \left[ \frac{\Omega}{s} + \mathcal{L} \left( \tilde{\alpha} \cdot \mathcal{L}^{-1} \left( \frac{\tilde{I}_k}{\mathcal{N}} \right) \cdot \mathcal{L}^{-1}(\tilde{S}_k) \right) + \xi \tilde{S}_k \right].$$

Similar expressions can be defined for all other compartments.

**Step 4:** For  $k = 1$ , the series becomes:

$$\tilde{Y}_1(s, p) = \frac{\tilde{Y}_0}{s} + \frac{\tilde{Y}_1}{s^{\omega+1}}.$$

Substitute these into the residual functions and multiply by  $s^{\omega+1}$  to remove denominators.

**Step 5:** Take the limit as  $s \rightarrow \infty$ :

$$\lim_{s \rightarrow \infty} (s^{\omega+1} \cdot LRes(\tilde{Y}_1(s, p))) = 0.$$

This generates an algebraic system that can be solved for the coefficients  $\tilde{Y}_1$ .

**Step 6:** Solving the system, we obtain:

$$\begin{aligned}\tilde{S}_1 &= \Lambda - \xi \tilde{S}_0 - \tilde{\alpha} \tilde{S}_0 \frac{\tilde{I}_0}{\mathcal{N}}, \\ \tilde{E}_1 &= \tilde{\alpha} \tilde{S}_0 \frac{\tilde{I}_0}{\mathcal{N}} - (\xi + \tilde{\eta}) \tilde{E}_0, \\ \tilde{I}_1 &= \tilde{\eta} \sigma \tilde{E}_0 - (\xi + \lambda + \rho + \sigma) \tilde{I}_0, \\ \tilde{H}_1 &= (\sigma) \tilde{I}_0 - (\xi + \tilde{\theta} + \tau) \tilde{H}_0, \\ \tilde{R}_1 &= \lambda \tilde{I}_0 + \tilde{\theta} \tilde{H}_0 - \xi \tilde{R}_0, \\ \tilde{D}_1 &= \rho \tilde{I}_0 + \tau \tilde{H}_0.\end{aligned}$$

**Step 7:** The same approach can be used recursively to compute the higher-order coefficients  $\tilde{X}_n$  for  $n > 1$ .

### Solution of fuzzy-fractional cholera model

We consider the cholera disease system expressed in fuzzy-fractional form as given in equation (8), where the model parameters are fuzzified as described in equation (7), subject to the following initial conditions.

$$\tilde{S}(0) = 39030914, \quad \tilde{E}(0) = 0, \quad \tilde{I}(0) = 8543, \quad \tilde{H}(0) = 253, \quad \tilde{R}(0) = 0, \quad \tilde{D}(0) = 329.$$

### Results and discussion

In this paper, we analyzed the transmission dynamics of the SEIHRD cholera model by examining the effects of key epidemiological parameters, the role of fractional-order derivatives, and the incorporation of fuzzy uncertainty. The graphical simulations and contour plots provide insights into how different factors influence the evolution of each compartment in the model.

Sensitivity analysis was performed by perturbing baseline parameter values by  $\pm 10\%$  to assess their relative influence on cholera dynamics. The results revealed that the transmission rate  $\alpha$  is the most sensitive parameter. Figure 2 shows that even a small increase in  $\alpha$  significantly elevates the epidemic peak, emphasizing the importance of limiting exposure to contaminated water sources and improving sanitation practices.

Figure 3 demonstrates the effect of the recovery rate  $\lambda$ . As  $\lambda$  increases, the number of infected individuals declines more rapidly, indicating quicker recovery and shorter infectious periods. This highlights the critical role of timely medical care, oral rehydration therapy, and antibiotics in reducing the spread of cholera.

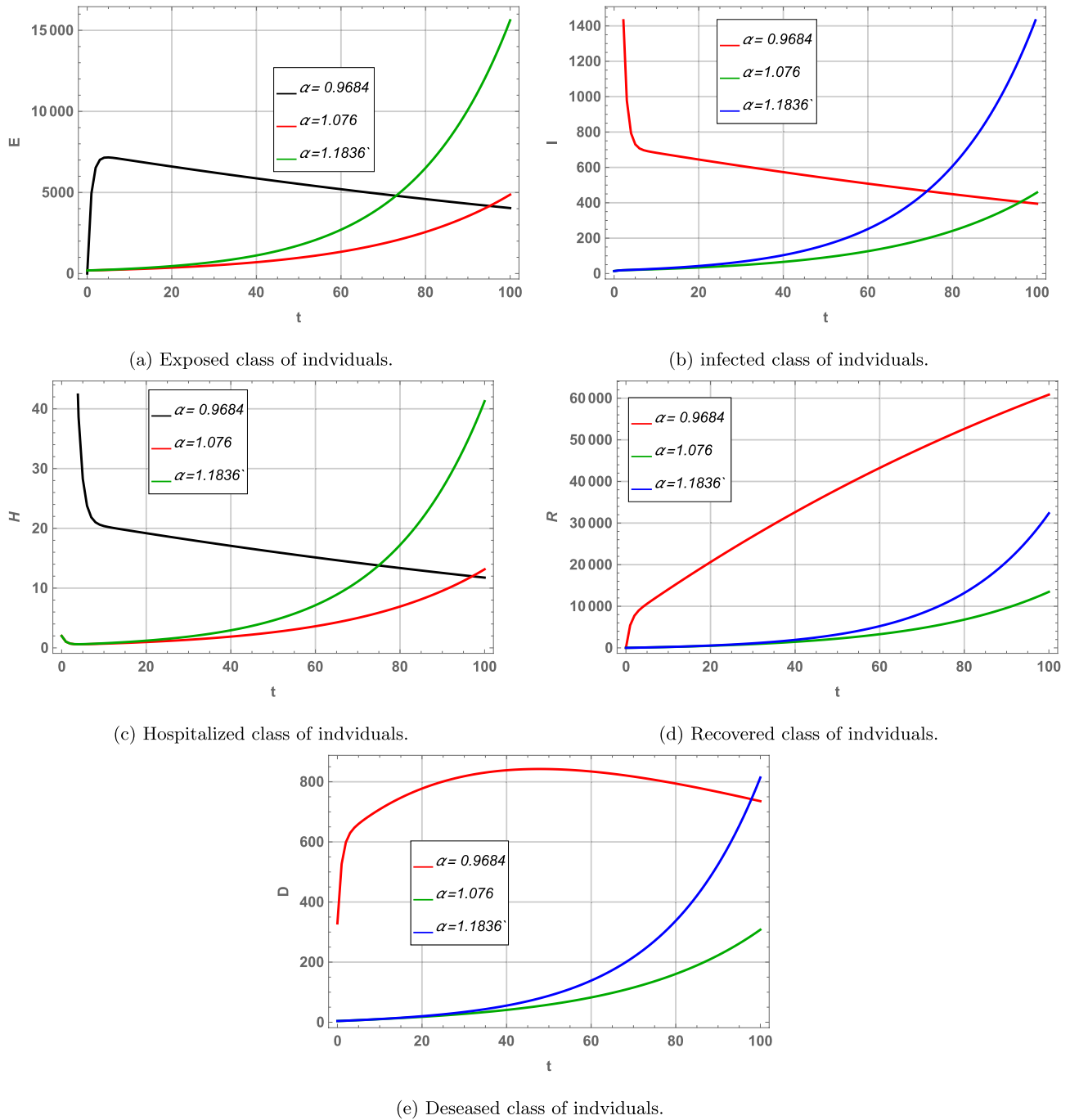
Figure 4 illustrates the impact of the hospitalization rate  $\sigma$  of infectious individuals. Higher values of  $\sigma$  transfer more patients from the infectious to the hospitalized class, thereby reducing immediate community-level transmission. This finding underscores the importance of hospital capacity, rapid admission, and isolation measures in containing cholera outbreaks.

Figure 5 presents the effect of the recovery rate of hospitalized individuals, denoted by  $\theta$ . Increasing  $\theta$  leads to faster discharges and reduces the burden on healthcare facilities. This demonstrates that improved treatment protocols and effective patient management are essential for minimizing mortality and ensuring quicker reintegration of patients into the susceptible or recovered population.

Figures 6, 7, 8, 9, 10 and 11 provide comparative contour plots of all compartments of the SEIHRD cholera model under different modeling approaches: fuzzy (lower and upper bounds), fractional, and fuzzy-fractional (lower and upper bounds). The fuzzy-only model captures uncertainty arising from imprecise epidemiological parameters, as reflected in the gap between the lower and upper bounds. By contrast, the fractional model incorporates memory effects but produces crisp trajectories, thus ignoring parameter uncertainty. The hybrid fuzzy-fractional model integrates both features, with smoother and narrower bounds compared to the purely fuzzy case, indicating improved robustness and predictive stability. Across all compartments (susceptible, exposed, infected, hospitalized, recovered, and deceased), the fuzzy-fractional approach provides a more realistic and flexible representation of cholera dynamics, especially under uncertain or incomplete data. These findings confirm that combining fractional calculus with fuzzy parameterization enhances interpretability and yields more reliable bounds for epidemic outcomes.

To the best of our knowledge, no prior study has investigated cholera dynamics using a hybrid fuzzy-fractional framework. Classical deterministic SEIHRD models assume precise parameters and lack memory effects, while fractional-order models incorporate history dependence but ignore uncertainty. Conversely, fuzzy epidemic models address uncertainty but neglect memory-driven processes. Our proposed hybrid fuzzy-fractional approach combines both features, offering a more robust and realistic description of cholera transmission, particularly when data are uncertain or incomplete.

Overall, the combined use of integer-order, fractional-order, and fuzzy-fractional analyses provides a comprehensive and reliable understanding of the SEIHRD cholera model. The  $\pm 10\%$  sensitivity analysis confirmed that the transmission and recovery rates are the most influential parameters. The fractional-order formulation revealed the importance of memory-driven dynamics, while the fuzzy framework successfully



**Figure 2.** Effect of  $\alpha$  on cholera model over time  $t$  (in days).

accounted for parameter uncertainty. Together, these approaches enhance the reliability of the model and provide valuable guidance for designing effective control and intervention strategies against cholera.

Despite its strengths, the fuzzy-fractional SEIHRD framework also presents several challenges. Underreporting and data ambiguity complicate the accurate estimation of key epidemiological characteristics, necessitating the use of fuzzy numbers. The inclusion of fractional-order derivatives further increases mathematical complexity due to the memory-dependent nature of disease progression. Moreover, ensuring biological realism while conducting stability and sensitivity analyses is particularly challenging when multiple compartments, such as hospitalized and deceased individuals, are included. Additionally, generating fuzzy-fractional contour plots and adjusting parameters increases computational demands, making careful interpretation essential for real-world applications. Nevertheless, the hybrid fuzzy-fractional approach provides a more robust and accurate depiction of cholera dynamics, offering valuable insights for planning and optimizing intervention strategies.

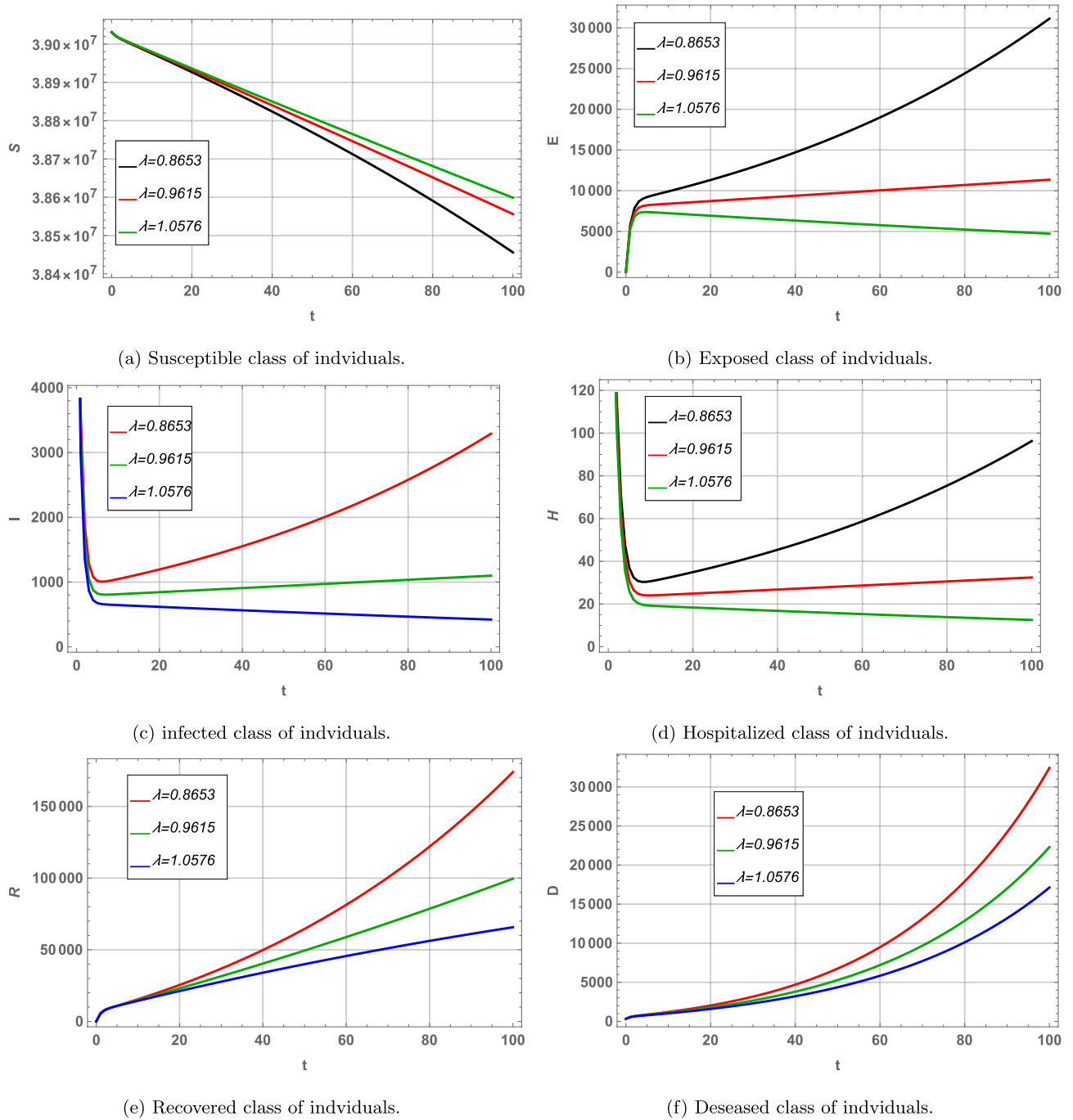


**Figure 3.** Effect of  $\lambda$  on cholera model over time  $t$  (in days).

### Conclusion

Cholera remains a persistent global health threat due to its rapid transmission, high morbidity, and frequent occurrence in regions with inadequate water sanitation and healthcare facilities. To capture these complexities, we developed a fractional-order SEIHRD epidemiological model enriched with fuzzy parameters. Calibrated using WHO outbreak data, the model incorporates Triangular fuzzy numbers to address parameter uncertainty and employs the Laplace Residual Power Series Method (LRPSM) to solve the fuzzy-fractional system effectively. Stability analysis confirmed that the system remains stable when  $\mathcal{R}_0 < 1$ , while simulations revealed the parameters most influential in cholera transmission, highlighting the roles of fractional order and fuzzy bounds.

By integrating fuzzy logic, fractional calculus, and sensitivity analysis within a single framework, the study provides a versatile tool for understanding cholera dynamics. The findings emphasize the importance of strengthening hospitalization and treatment facilities to reduce mortality and improving water sanitation to limit exposure. Practical recommendations are offered for policymakers in Angola and similar contexts, including

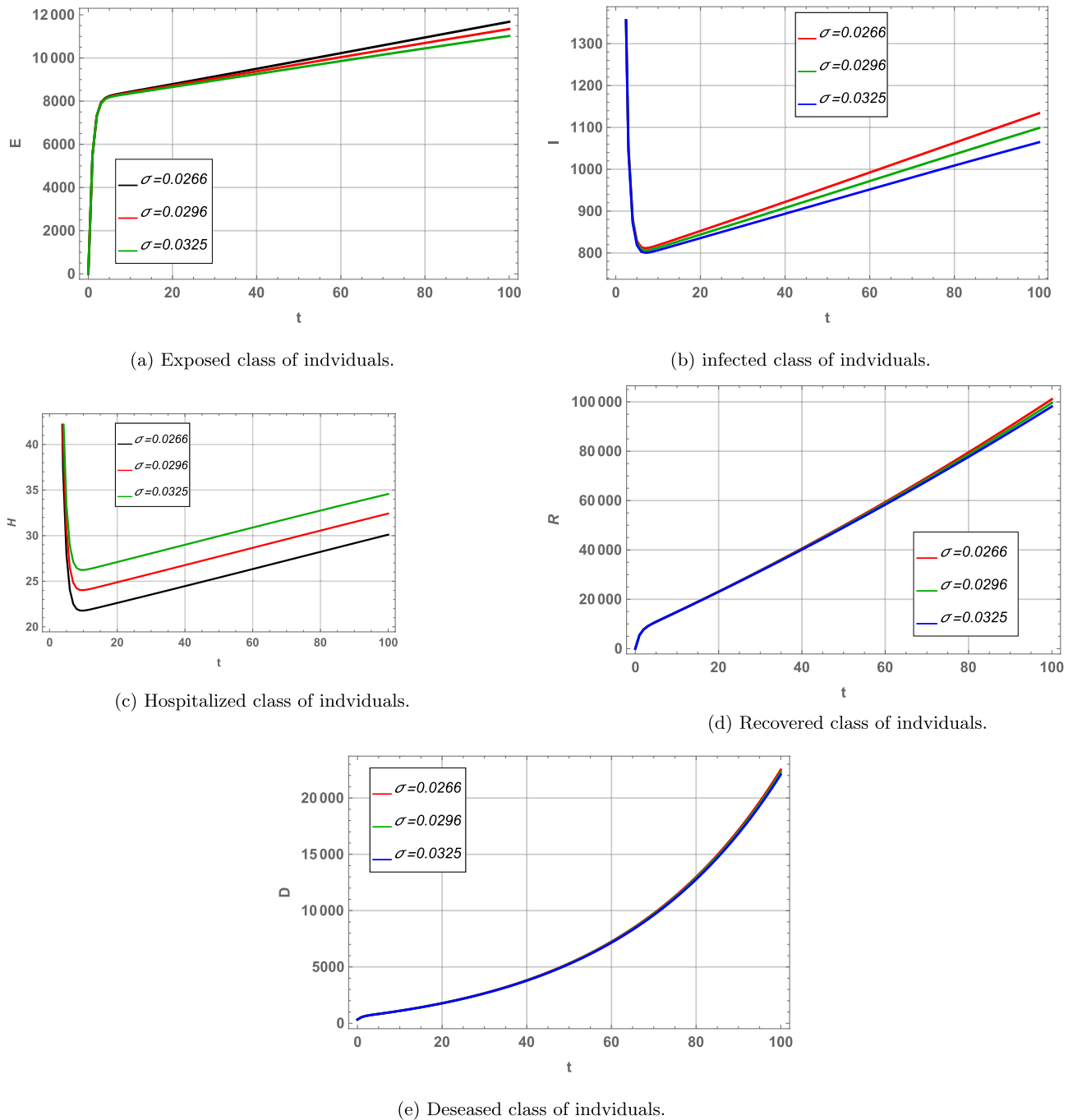
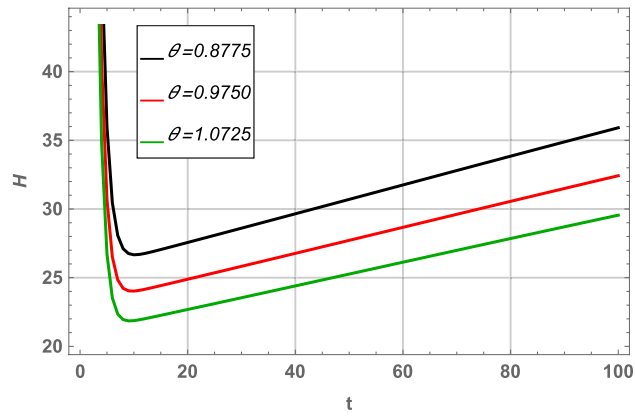


**Figure 4.** Effect of  $\sigma$  on cholera model over time  $t$  (in days).

prioritizing rapid case detection, expanding treatment capacity, and promoting community-level interventions to curb both disease spread and cholera-related fatalities.

The LRPS method demonstrated clear advantages, such as effectively managing fractional dynamics and fuzzy uncertainty and yielding rapidly convergent approximations. However, its accuracy depends on truncation choices, and computational costs may rise with highly nonlinear systems or large datasets. Despite these limitations, the method remains a valuable analytical tool, with potential for further refinement and broader applications in real-world epidemiological modeling.

In future work, this framework can be extended to other waterborne diseases beyond cholera to test its broader applicability. Additionally, applying the model to multi-country outbreak datasets would allow for comparative analysis across diverse epidemiological settings. Further refinements of the LRPS method may enhance computational efficiency, particularly for large-scale or highly nonlinear systems. Finally, integrating the model with public health intervention strategies could provide deeper insights into effective control measures and policy planning.



Hospitalized class of individuals.

**Figure 5.** Effect of  $\theta$  on Cholera model over time  $t$  (in days).

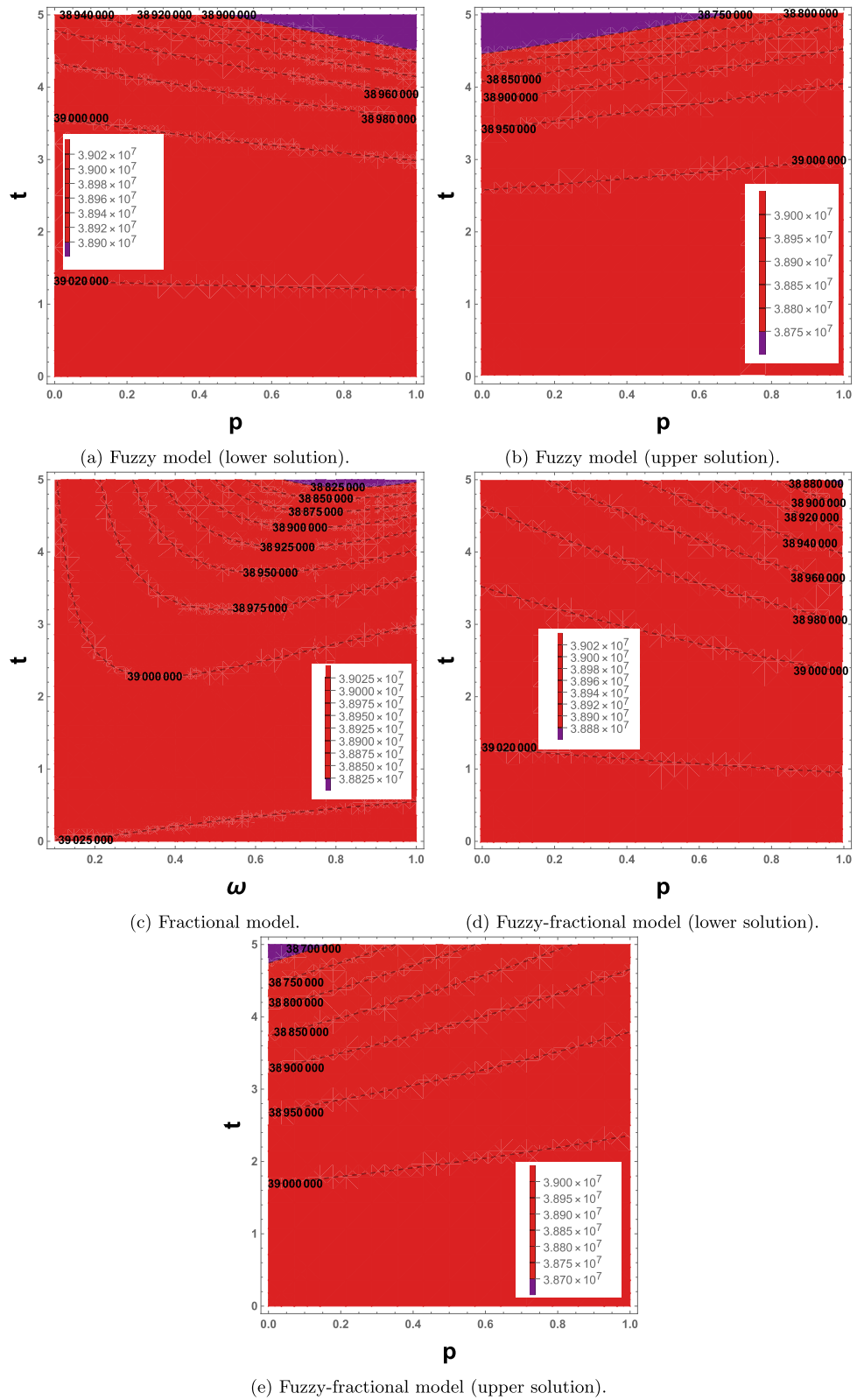


**Figure 6.** Comparative contour plots of the susceptible population in the cholera SEIHRD model. The panels show (a) fuzzy model (lower solution), (b) fuzzy model (upper solution), (c) fractional model, (d) fuzzy-fractional model (lower solution), and (e) fuzzy-fractional model (upper solution).

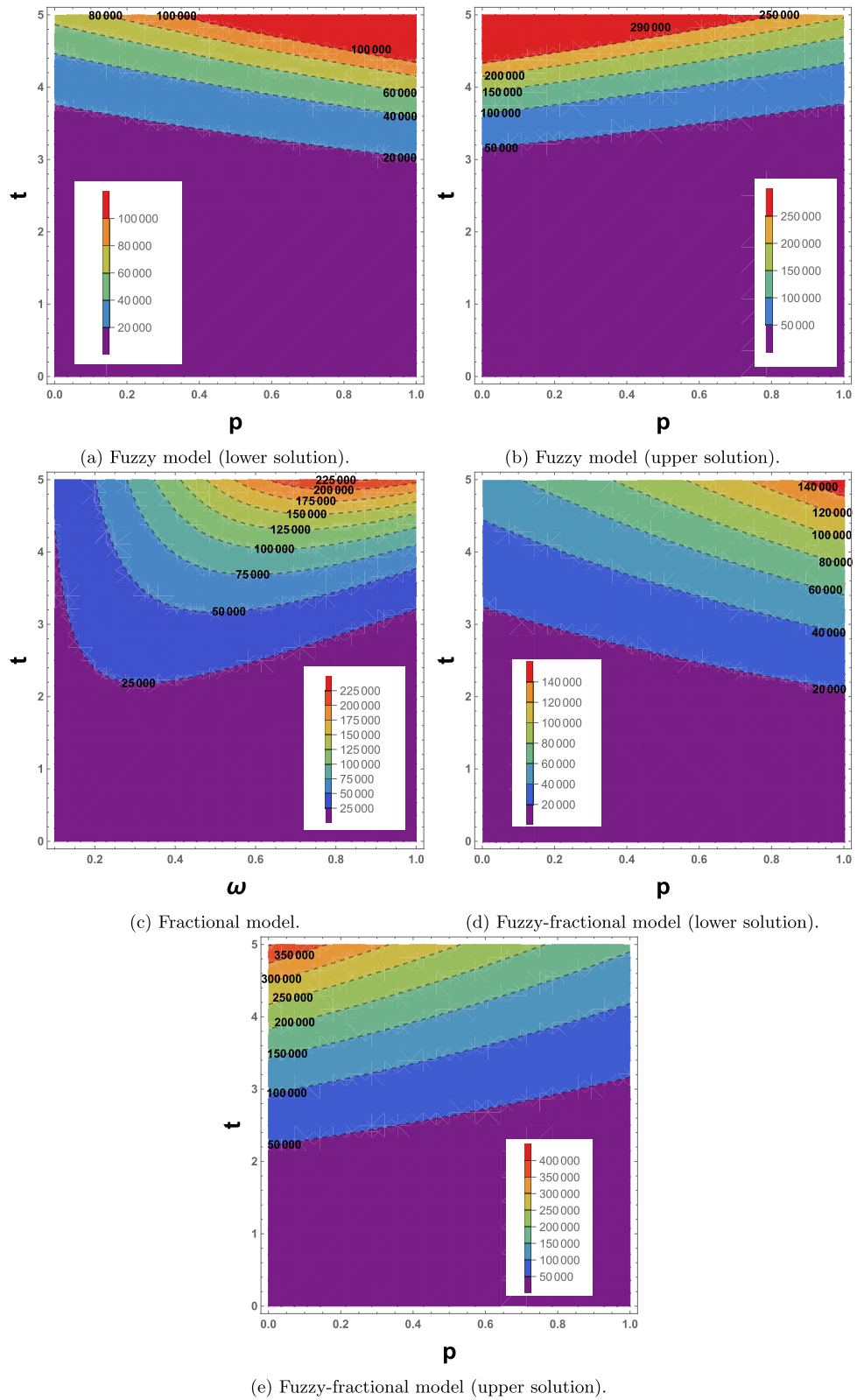


**Figure 7.** Comparative contour plots of the exposed population in the cholera SEIHRD model. The panels show (a) fuzzy model (lower solution), (b) fuzzy model (upper solution), (c) fractional model, (d) fuzzy-fractional model (lower solution), and (e) fuzzy-fractional model (upper solution).

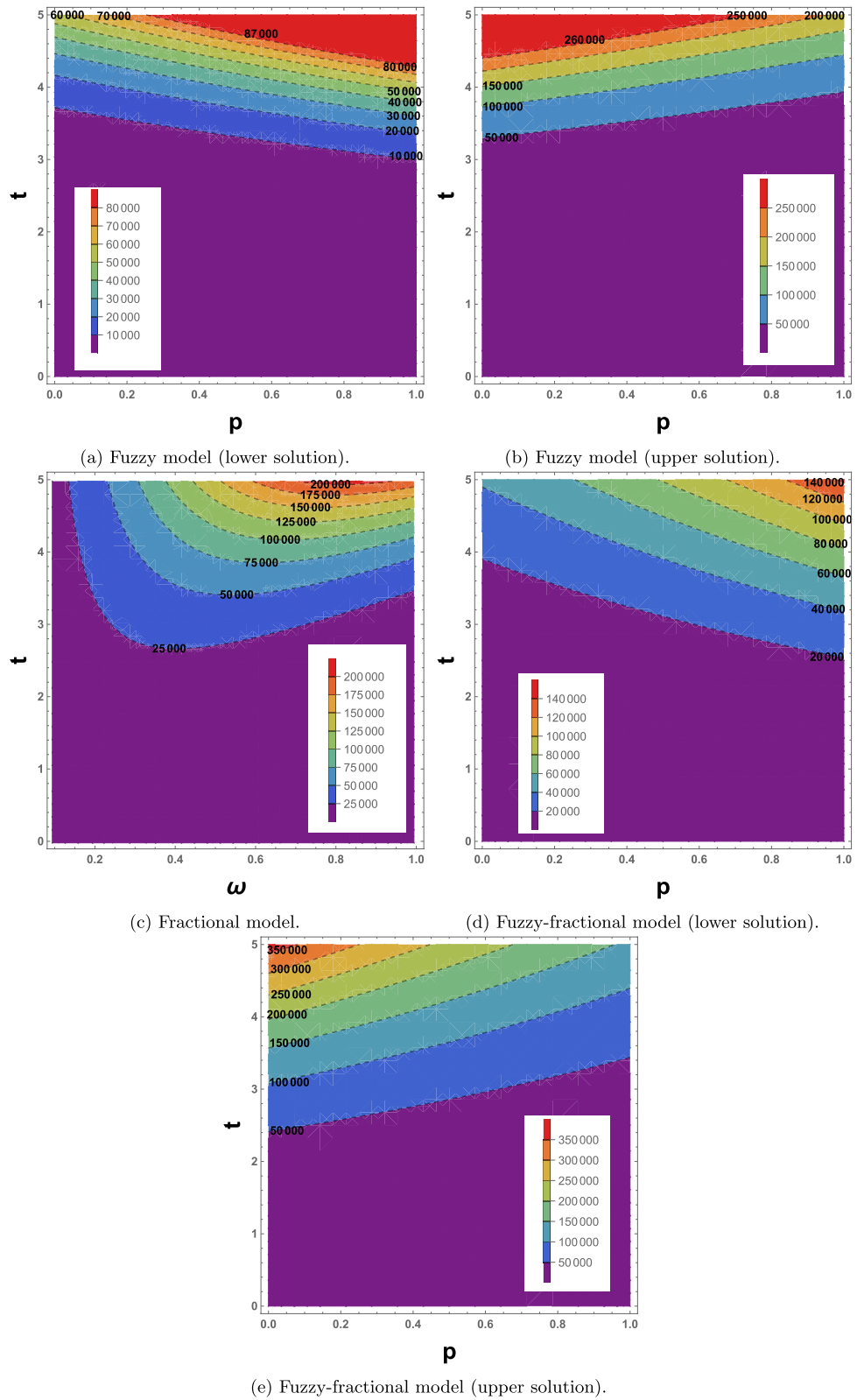


**Figure 8.** Comparative contour plots of the infected population in the cholera SEIHRD model. The panels show (a) fuzzy model (lower solution), (b) fuzzy model (upper solution), (c) fractional model, (d) fuzzy-fractional model (lower solution), and (e) fuzzy-fractional model (upper solution).

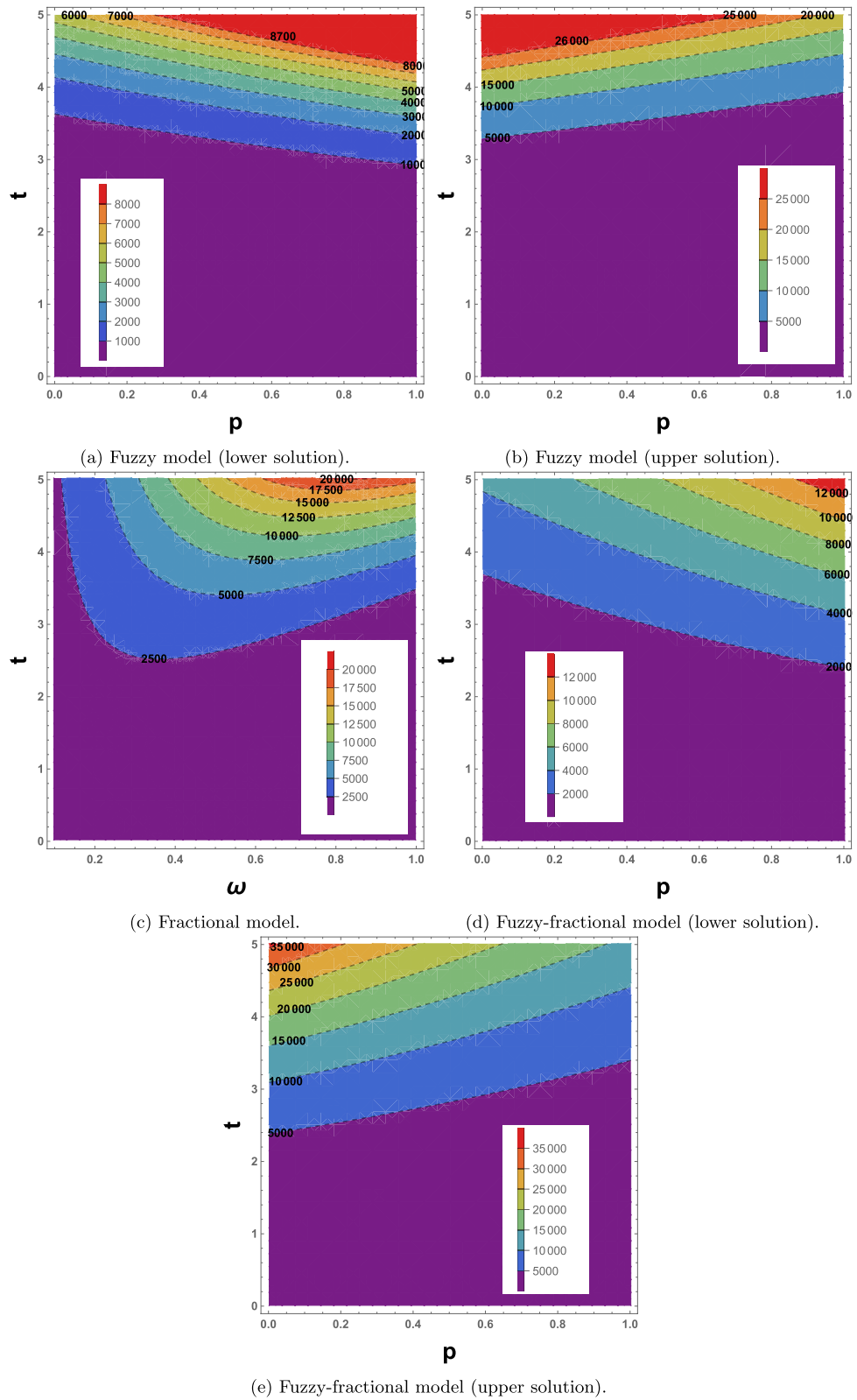


**Figure 9.** Comparative contour plots of the hospitalized population in the cholera SEIHRD model. The panels show (a) fuzzy model (lower solution), (b) fuzzy model (upper solution), (c) fractional model, (d) fuzzy-fractional model (lower solution), and (e) fuzzy-fractional model (upper solution).

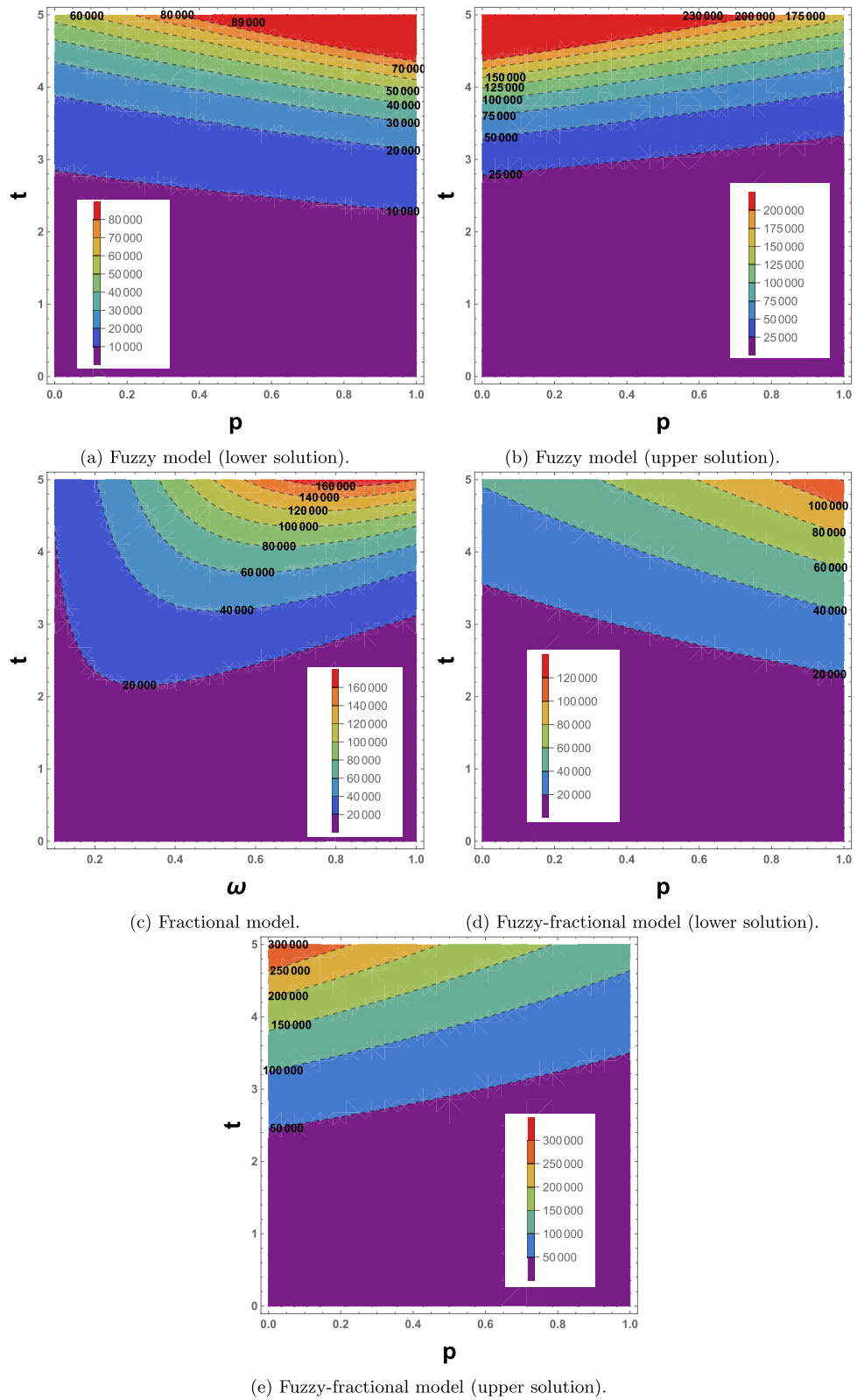


**Figure 10.** Comparative contour plots of the recovered population in the cholera SEIHRD model. The panels show (a) fuzzy model (lower solution), (b) fuzzy model (upper solution), (c) fractional model, (d) fuzzy-fractional model (lower solution), and (e) fuzzy-fractional model (upper solution).

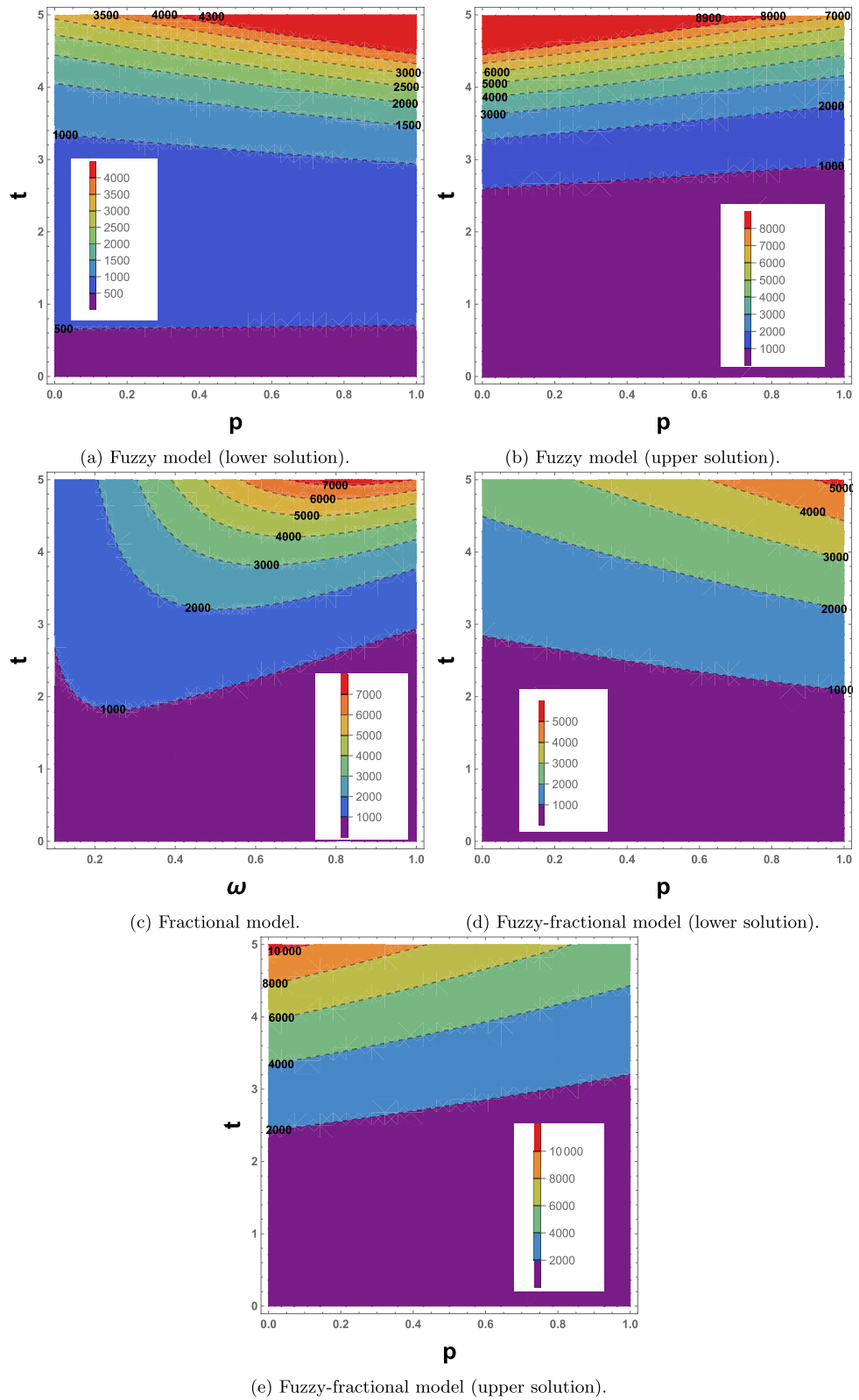


**Figure 11.** Comparative contour plots of the deceased population in the cholera SEIHRD model. The panels show (a) fuzzy model (lower solution), (b) fuzzy model (upper solution), (c) fractional model, (d) fuzzy-fractional model (lower solution), and (e) fuzzy-fractional model (upper solution).

## Data availability

All data generated or analysed during this study are included in this published article.

Received: 13 September 2025; Accepted: 22 October 2025

Published online: 01 December 2025

## References

1. Marwa, Y. M., Mbalawata, I. S., Mwalili, S., & Charles, W. M. Stochastic dynamics of cholera epidemic model: Formulation, analysis and numerical simulation. *J. Appl. Math. Phys.* **07**(05), 1097–1125 (2019).
2. Eurien, D., et al. Cholera outbreak caused by drinking unprotected well water contaminated with faeces from an open storm water drainage: kampala city, uganda, january 2019. *BMC Infect. Dis.* **21**(1) (2021).
3. Sack, D. A., et al. Cholera. *The Lancet* **363**(9404):223–233 (2004).
4. Faruque, S. M., John Albert, M. & Mekalanos, J. J. Epidemiology, genetics, and ecology of toxigenic vibrio cholerae. *Microbiol. Mol. Biol. Rev.* **62**(4), 1301–1314 (1998).
5. Devault, A. M., et al. Second-pandemic strain of vibrio cholerae from the philadelphia cholera outbreak of 1849. *N. Engl. J. Med.* **370**(4), 334–340 (2014).
6. Siddique, A. K., & Cash, R. *Cholera outbreaks in the classical biotype era*, pages 1–16 (Springer Berlin Heidelberg, 2013).
7. Camacho, A., et al. Cholera epidemic in yemen, 2016–18: an analysis of surveillance data. *Lancet Global Health* **6**(6), e680–e690 (2018).
8. Report. Cholera-global situation, world health organization - disease outbreak news, WHO, 2022.
9. Cai, L., Fan, G., Yang, C. & Wang, J. Modeling and analyzing cholera transmission dynamics with vaccination age. *J. Franklin Inst.* **357**(12), 8008–8034 (2020).
10. Report. Cholera vaccines: who position paper who - wkly epidemiol rec, 2010. WHO, 2010.
11. Clemens, J. Field trial of oral cholera vaccines in bangladesh: results from three-year follow-up. *The Lancet* **335**(8684), 270–273 (1990).
12. Ali, M., et al. Herd protection by a bivalent killed whole-cell oral cholera vaccine in the slums of kolkata, india. *Clin. Infect. Dis.* **56**(8), 1123–1131 (2013).
13. Kermack, W. O. & McKendrick, A. G. Contributions to the mathematical theory of epidemics-I. *Bull. Math. Biol.* **53**(1–2), 33–55 (1991).
14. Shuai, Z., & van den Driessche, P. Modelling and control of cholera on networks with a common water source. *J. Biol. Dyn.* **9**(sup1), 90–103 (2014).
15. Rajendran, K., et al. Influence of relative humidity in vibrio cholerae infection: a time series model. *Indian J. Med. Res.* **133**(2), 138–145 (2011).
16. Appiah Osei, B., et al. Utilisation of social media by international tourists to ghana. *Anatolia* 1–11 (2018).
17. Cui, Q., et al. Bifurcation and controller design of 5d bam neural networks with time delay. *Int. J. Numer. Model. Electron. Netw. Dev. Fields* **37**(6) (2024).
18. Ratchford, C. & Wang, J. Modeling cholera dynamics at multiple scales: environmental evolution, between-host transmission, and within-host interaction. *Math. Biosci. Eng.* **16**(2), 782–812 (2019).
19. Bai, J., Yang, C., Wang, X. & Wang, J. Modeling the within-host dynamics of cholera: bacterial-viral-immune interaction. *J. Appl. Anal. Comput.* **11**(2), 690–710 (2021).
20. Zadeh, L. A. Fuzzy sets. *Inf. Control* **8**(3), 338–353 (1965).
21. Mondal, P. K., Jana, S., Haldar, P., & Kar, T. K. Dynamical behavior of an epidemic model in a fuzzy transmission. *Int. J. Uncert. Fuzz. Knowl. Based Syst.* **23**(05), 651–665 (2015).
22. De Barros, L. C., Ferreira Leite, M. B. & Bassanezi, R. C. The si epidemiological models with a fuzzy transmission parameter. *Comput. Math. Appl.* **45**(10–11), 1619–1628 (2003).
23. Butzer, P. L., & Westphal, U. *An introduction to fractional calculus*, pages 1–85. World scientific (2000).
24. Qayyum, M., Fatima, Q., Akgül, A., & Khan Hassani, M. Modeling and analysis of dengue transmission in fuzzy-fractional framework: a hybrid residual power series approach. *Sci. Rep.* **14**(1) (2024).
25. Fatima, Q. et al. Dynamical analysis of fractional hepatitis b model with gaussian uncertainties using extended residual power series algorithm. *Sci. Rep.* **15**(1) (2025).
26. Qayyum, M., Ahmad, E. & Ali, M. R. New solutions of time-fractional cancer tumor models using modified he-laplace algorithm. *Heliyon* **10**(14), e34160 (2024).
27. Aguegboh, N. S. et al. A novel approach to modeling malaria with treatment and vaccination as control strategies in Africa using the Atangana-Baleanu derivative. *Model. Earth Syst. Environ.* **11**(2) (2025).
28. Stanley Aguegboh, N. et al. Existence and uniqueness of solution for a fractional hepatitis b model. *Comput. Math. Biophys.* **13**(1) (2025).
29. Xu, C. et al. Mathematical analysis and dynamical transmission of seirsr model with different infection stages by using fractional operator. *Int. J. Biomath.* (2025).
30. Yunus, A. O., & Olayiwola, M. O. Mathematical modeling of malaria epidemic dynamics with enlightenment and therapy intervention using the laplace-adomian decomposition method and caputo fractional order. *Franklin Open* **8**, 100147 (2024).
31. Yunus, A. O., & Olayiwola, M. O. Simulation of a novel approach in measles disease dynamics models to predict the impact of vaccinations on eradication and control. *Vacunas* **26**(2), 100385 (2025).
32. Venkatesh, A., et al. A fractional mathematical model for vaccinated humans with the impairment of monkeypox transmission. *Eur. Phys. J. Spec. Top.* **234**(8), 1891–1911 (2024).
33. Manivel, M., Venkatesh, A., & Kumawat, S. Numerical simulation for the co-infection of monkeypox and hiv model using fractal-fractional operator. *Model. Earth Syst. Environ.* **11**(3) (2025).
34. Khan, Z. A., Khan, A., Abdeljawad, T., & Khan, H. Computational analysis of fractional order imperfect testing infection disease model. *Fractals* **30**(05) (2022).
35. Kumar, S., Kumar, R., Agarwal, R. P. & Samet, B. A study of fractional lotka-volterra population model using haar wavelet and adams-bashforth-moulton methods. *Math. Methods Appl. Sci.* **43**(8), 5564–5578 (2020).
36. Ghanbari, B., Kumar, S., & Kumar, R. A study of behaviour for immune and tumor cells in immunogenetic tumour model with non-singular fractional derivative. *Chaos Solitons Fract.* **133**, 109619 (2020).
37. Khan, A. et al. Digital analysis of discrete fractional order cancer model by artificial intelligence. *Alex. Eng. J.* **118**, 115–124 (2025).
38. Qayyum, M., Ahmad, E., Tahir, A. & Acharya, S. Modeling and analysis of the fuzzy-fractional chaotic financial system using the extended he-mohand algorithm in a fuzzy-caputo sense. *Int. J. Intell. Syst.* **2023**, 1–15 (2023).
39. Eriqat, T., El-Ajou, A., Oqielat, M. N., Al-Zhour, Z. & Momani, S. A new attractive analytic approach for solutions of linear and nonlinear neutral fractional pantograph equations. *Chaos Solitons Fract.* **138**, 109957 (2020).
40. Gul, N. et al. The dynamics of fractional order hepatitis b virus model with asymptomatic carriers. *Alex. Eng. J.* **60**(4), 3945–3955 (2021).

41. van den Driessche, P. & Watmough, J. Reproduction numbers and sub-threshold endemic equilibria for compartmental models of disease transmission. *Math. Biosci.* **180**(1–2), 29–48 (2002).
42. Report. Cholera angola world health organization disease outbreak news. *WHO*, (2025).

### Acknowledgement

The authors extend his appreciation to the Deanship of Scientific Research at King Khalid University for funding this work through research groups program under Grant No. R.G.P2/307/46.

### Author contributions

Qursam Fatima: Performed the experiment; Analyzed and interpreted the data; Wrote the paper. Mubashir Qayyum: Conceived and designed the experiments; Supervision; Analyzed and interpreted the data; Contributed reagents, materials, analysis tools or data; Wrote the paper. Omar Khan: Analyzed and Interpreted the data; Validated results; Review the final draft of paper. Abdou Al zubaidi: Analyzed and Interpreted the data; materials, analysis tools or data; Review the final draft of paper. Syed Tauseef Saeed: Analyzed and Interpreted the data; materials, analysis tools or data; Review the final draft of paper. Jihad Younis: Analyzed and Interpreted the data; materials, analysis tools or data; Review the final draft of paper.

### Funding

The authors extends his appreciation to the Deanship of Scientific Research at King Khalid University for funding this work through research groups program under Grant No. R.G.P2/307/46.

### Declarations

#### Competing interests

The authors declare no competing interests.

#### Additional information

**Correspondence** and requests for materials should be addressed to J.Y.

**Reprints and permissions information** is available at [www.nature.com/reprints](http://www.nature.com/reprints).

**Publisher's note** Springer Nature remains neutral with regard to jurisdictional claims in published maps and institutional affiliations.

**Open Access** This article is licensed under a Creative Commons Attribution-NonCommercial-NoDerivatives 4.0 International License, which permits any non-commercial use, sharing, distribution and reproduction in any medium or format, as long as you give appropriate credit to the original author(s) and the source, provide a link to the Creative Commons licence, and indicate if you modified the licensed material. You do not have permission under this licence to share adapted material derived from this article or parts of it. The images or other third party material in this article are included in the article's Creative Commons licence, unless indicated otherwise in a credit line to the material. If material is not included in the article's Creative Commons licence and your intended use is not permitted by statutory regulation or exceeds the permitted use, you will need to obtain permission directly from the copyright holder. To view a copy of this licence, visit <http://creativecommons.org/licenses/by-nc-nd/4.0/>.

© The Author(s) 2025, corrected publication 2025